Title
EVIDENCE FOR ORBITAL DISPERSION IN THE FRAGMENTATION OF 160 AT 90 AND 120 MeV/NUCLEON

Author
Van Bibber, K.

Publication Date
1979-03-01

Submitted to Physical Review Letters

LBL-8939
Preprint

EVIDENCE FOR ORBITAL DISPERSION IN THE FRAGMENTATION OF ^{16}O AT 90 AND 120 MeV/NUCLEON

K. Van Bibber, D. L. Hendrie, D. K. Scott, H. H. Wieman
L. S. Schroeder, J. V. Geaga, S. A. Chessin, R. Treuhaft,
J. Y. Grossiord, J. O. Rasmussen and C. Y. Wong

March 1979

Prepared for the U. S. Department of Energy
under Contract no. W-7405-ENG-48

DISCLAIMER

EVIDENCE FOR ORBITAL DISPERSION IN THE FRAGMENTATION OF ^{16}O AT 90 and 120 MEV/NUCLEON

K. Van Bibber, D. L. Hendrie, D. K. Scott, H. H. Wieman
L. S. Schroeder, J. V. Geaga, S. A. Chessin, R. Treuhaft,
J. Y. Grossiord†, and J. O. Rasmussen

Lawrence Berkeley Laboratory
University of California
Berkeley, California 94720

and

C. Y. Wong

Oak Ridge National Laboratory
Oak Ridge, Tennessee 37830

March 1979

Abstract:

The parallel and transverse momentum distributions have been measured for fragments of $Z \geq 3$ produced by the fragmentation of ^{16}O at 90 and 120 MeV/nucleon. A strong anisotropy is observed with $\sigma_{p_\perp} \gtrsim 200$ MeV/c for all fragments, which can be explained by considering the dispersion due to orbital deflection of the projectile prior to breakup.

The questions of reaction mechanism in projectile fragmentation has been long standing. At relativistic energies with ^{12}C and ^{16}O projectiles, both the abrasion-ablation calculations and models of projectile excitation followed by statistical decay adequately describe the isotope distributions.[1,2] Further, it has been pointed out that there is an exact formal degeneracy between such models with regards to the fragment momentum distributions.[3] Recent data for a heavier projectile and lower energy (^{40}Ar, 213 MeV/nucleon) however, seem to favor a fast abrasion stage from relative isotopic and elemental yields.[4] We report here in the first heavy fragment studies in the 100 MeV/nucleon region, an apparent anisotropy between $p_\perp$ and $p_\parallel$. Incorporating the dispersion due to orbital deflection of the ^{16}O projectile by the combined Coulomb-nuclear field of the target with the usual dispersion due to the Fermi motion, we find good agreement with the $p_\perp$ distributions. Although the present data also support either the abrasion-ablation model or the assumption of projectile excitation followed by statistical decay far from the target nucleus, better measurements at smaller $p_\perp$ could discriminate between them and potentially prove to be a new tool for probing the interaction potential in the nuclear interior.

The ^{16}O beam was extracted from the Bevalac with an energy of typically 150 MeV/A and an intensity $\approx 10^9$/pulse. After passing through a carbon degrader and subsequent momentum analysis and cleanup, the average intensities and midtarget energies were (for 150 MeV/A extraction) $\approx 5 \times 10^7$/pulse at 92.5±2 MeV/A and $\approx 10^8$/pulse at 117.5±2 MeV/A. Targets of thicknesses up to 235 mg/cm^2 Al and 500 mg/cm^2 Au were bombarded, and fragments of Z = 3-9, A = 6-17 were detected in a multi-element silicon-

germanium telescope, the ΔE stack consisting of two 5 mm Si detectors at 120 MeV/A and two 1 mm Si detectors at 90 MeV/A. The residual E detector was a 1.3 cm Ge crystal. A silicon veto detector behind the telescope proved reasonably effective in eliminating events which underwent secondary fragmentation in the germanium crystal itself; this effect however was never greater than 10%. A circular lead collimator subtended 0.9° full width at 1.6 m, and a helium bag was placed between the target and detector. At each angle, the "target out" spectrum was measured and corrected for.

Double differential cross sections $d^2\sigma/d\Omega dE$ were measued for each isotope at each angle (2.5°, 4°, 6°, 8° at 92.5 MeV/A; 2.5°, 4°, 7° at 117.5 MeV/A.) The energy spectra were narrow, essentially Gaussian, with a mean energy downshifted by ≈ 10 MeV/A from the beam velocity.[5] We fit the energy spectra and angular distributions assuming a Gaussian distribution in both $p_\parallel$ and $p_\perp$ in the projectile frame of reference:

$$P(\vec{p}) \propto \exp\left(- \frac{p_\parallel^2}{2\sigma_{p_\parallel}^2} - \frac{p_\perp^2}{2\sigma_{p_\perp}^2} \right). \qquad (1)$$

The distributions of $\sigma_{p_\parallel}$ as a function of fragment mass F are in good agreement with the parabolic form $\sigma_{p_\parallel}^2 = \sigma_o^2 \; F(A-F)/(A-1)$ expected from momentum conservation and experimentally observed at higher energies.[3,6] A and F are the projectile and fragment atomic numbers respectively. At 92.5 MeV/A we find σ_o = 80 MeV/c for the Au target, and 86 MeV/c for the Al, in good agreement with the value of 86 MeV/c found at 2.1 GeV/A, averaged over many targets.[6]

The situation with the distributions of $\sigma_{p_\perp}$ is rather different. An inspection of the angular distributions (see Fig. 1) reveals that they are significantly broader than expected from the Fermi motion alone. The solid curves are the best fits in $\sigma_{p_\perp}$ from Eq. (1); the dashed curves pertain to σ_o = 86 MeV/c. Figure 2 shows the ensemble of all transverse momentum widths, which are nearly all in excess of 200 MeV/c with an overall systematic increase with fragment mass. This behaviour is in sharp contrast with that at 1.05 and 2.1 GeV/A where $\sigma_{p_\parallel} = \sigma_{p_\perp}$ to within 10%.

The origin of these surprisingly large widths may be understood if one notes that the projectile is subject to an orbital deflection due to its interaction with the target nucleus before fragmentation takes place. The large fragmentation cross section implies that a wide range of impact parameters contribute to this process, and as different impact parameter will lead to different deflection angles, the orbital deflection gives an additional dispersion of the transverse momentum. Clearly the additional contribution to the width of $\sigma_{p_\perp}$ becomes more important the lower the energy of the projectile. Upon extending the derivations of Ref. 3 to include orbital deflection, we find.

$$\sigma^2_{p_\perp}(F) = \frac{F(A-F)}{A-1}\ \sigma_1^2 + \frac{F(F-1)}{A(A-1)}\ \sigma_2^2 \qquad (2)$$

where $\sigma_1^2 = \frac{1}{2} < \vec{p}^{\,2}_{I\perp} > = \sigma_o^2$ is the usual term due to the intrinsic nucleon motion, and $\sigma_2^2 = \frac{1}{2} < \vec{p}^{\,2}_{A\perp} >$ is the variance of transverse momentum of the projectile at the time of fragmentation.

The quality of the two-parameter fits according to Eq. (2) is evidently good. Table I contains the summary of the fitted and calculated values of σ_2. Fitting the experimental $\sigma_{p_\perp}(F)$ according to Eq. 2,

we fix σ_1 = 80, 86 MeV/c. However when σ_1 is also allowed to be a free parameter, its value is equal within errors to $\sigma_{p_\parallel}$, convincing evidence that the functional form of Eq. (2) contains the essential physics. In Fig. 3, panels (a)-(c) show the best two parameter fit (σ_1 not constrained; values in Table I); panel (d) shows the family of curves corresponding to one value of σ_1, and values of σ_2 ranging from 0 to 300 MeV/c.

Having thus understood the average behavior of the widths, we seek a more detailed description of the angular distributions. We consider a simple model in which the projectile is first deflected through the Coulomb-nuclear potential and subsequently fragments. The angular distribution of any fragment is obtained by folding the projectile angular distribution from the classical deflection function with the fragment momentum distribution due to the Fermi motion. The nuclear potential is taken to be of the Woods-Saxon form with radius parameter r_o = 1.2 fm, diffusivity a = 0.6 fm, and the well depth to be determined. The behaviour of Θ (b) for small b is certainly not very reliable owing to the uncertainty in the Coulomb potential inside the nucleus. Both point charge and parabolic Coulomb potentials were used and the main difference appears to be at small angles for which no experimental data points are available. The only other input to the calculation is the fraction of the total cross section which appears as fragmentation, $f = \sigma_{frag}/\sigma_{tot}$. This value, 0.6 ± 0.1 for both targets,[7] defines the range in impact parameter (b_1,R) over which the deflection function operates in a sharp cutoff representation (insert, Fig. 3). Here R is the sum of target and projectile radii, $R = r_o(A_1^{1/3}+A_2^{1/3})$. In terms of the deflection function the variance σ_2^2

is given by $\sigma_2^2 = \frac{1}{2} p_A^2 \int_{b_1}^{R} N(b) \sin^2 \Theta(b) db$ and $N(b) = 2b/(R^2-b_1^2)$ is the weighting factor for impact parameter. Implicit in that calculation is the assumption that the dispersion is principally refractive, or dynamic, rather than quantal; in the 100 MeV/A region, this can be shown to be reasonably satisfied.

The comparison of the experimental angular distributions with those resulting from the folding procedure (dotted line, Fig. 1) indicate that the shape of the angular distribution can be well reproduced by choosing a potential well depth of 65 MeV for the Al target and 85 MeV for Au, which are within the range of depths determined from optical model analyses. Two aspects of these calculations deserve comment. The first is that for the larger fragment masses, the angular distributions are predicted to peak at a non-zero angle. Second, we observe that while our choice of potentials reproduce the average falloff of the data with angle, the calculated angular distributions are slightly wider for the lighter fragments and narrower to the heavier fragments.

To examine to what degree this behavior may be due to an impact parameter dependence of the final fragment mass, we have alternatively performed these calculations assuming an abrasion-ablation mechanism. Thus instead of the entire range of impact parameters (b_1,R) contributing equally to the calculated dispersion, for all F weighted only by N(b), we now posit that the production of a fragment of mass F is associated with a mean impact parameter b_F. The b_F are calculated in the "clean-cut" geometry, and for each F the integration over impact parameters is weighted further by a realistic smearing function,[1] of Gaussian form with full width 2 fm and mean b_F. These calculations for the Au target

are depicted by the fine line in Fig. 1; the parabolic continuation of the Coulomb potential inside the nuclear interior has been employed. Although several difficult questions are left unaddressed in this simple approach, it is clear that such an impact parameter dependence would manifest itself most strikingly near 0°. On the other hand both the abrasion-ablation model and that of projectile excitation followed by decay far from the nuclear field of the target seem not to differ substantially in the tails of the angular distribution.

In summary, the large $\sigma_{p_\perp}$ observed in the fragmentation of ^{16}O in the vicinity of 100 MeV/A are well described by incorporating the dispersion due to orbital deflection of the projectile prior to fragmentation along with Fermi motion. The orbital dispersion is larger at 92.5 MeV/A than at 117.5 MeV/A as expected, and both experiment and theory diminish by the same ratio. The calculations (non-relativistic) for the case of ^{16}O + Au at 400 MeV/A predict σ_2 = 89 MeV/c, suggesting that by 1.05 GeV/A the orbital dispersion term will have vanished entirely, and isotropy recovered. With regards to data from the reaction ^{16}O + ^{208}Pb at 20 MeV/A, it seems that this analysis qualitatively accounts for similar discrepancies between $\sigma_{p_\parallel}$ and $\sigma_{p_\perp}$, although the orbital dispersion at that energy should be predominantly quantal rather than dynamic.[9] While present data cannot distinguish between excitation followed by decay far from the target, and abrasion-ablation mechanisms, measurements into 0° will be of greatest utility for reaction dynamics. Such measurements may prove to be a useful tool in probing the nucleus-nucleus potential for deep incursions of the target and projectile.

We thank the Bevatron operating crew for providing these low energy beams, and acknowledge useful discussions with Peter Linstrom, Douglas Greiner, Lance Wilson, Hank Crawfored, Erwin Friedlander and G. R. Satchler. The work was supported by the Nuclear Physics Division of the U.S. Department of Energy under contract No. W-7405-ENG-48 and Union Carbide.

REFERENCES AND FOOTNOTES

†Present address: Institut de Physique Nucléaire de Lyon, 43 Boulevard du 11 Novembre 1918, 69621 Villeurbanne, France.

1. J. Hüfner, K. Schäfer, B. Schürmann, Phys. Rev. C12, 1888 (1975).
2. V. K. Lukyanov, A. I. Titov, Phys. Lett. 57B, 10 (1975); J. Hüfner, C. Sander, G. Wolschin, Phys. Lett. 73B, 289 (1978).
3. A. S. Goldhaber, Phys. Lett. 53B, 306 (1974).
4. Y. P. Viyogi, T. J. M. Symons, P. Doll, D. E. Greiner, H. H. Heckman, D. L. Hendrie, P. J. Lindstrom, J. Mahoney, D. K. Scott, K. Van Bibber, G. D. Westfall, H. Wieman, H. J. Crawfore, C. McParland, C. K. Gelbke, Phys. Rev. Lett. 42, 33 (1979).
5. We refer here to the isotopes $A \leqslant 15$, as one does also observe nucleon pickup but with very small cross sections. For example the total cross section for Au(^{16}O,^{17}F) at 92.5 MeV/A is $\sim$ 1.2 mb.
6. D. E. Greiner, P. J. Lindstrom, H. H. Heckman, Bruce Cork, F. S. Bieser, Phys. Rev. Lett. 35, 152 (1975).
7. Isotope production cross sections as well as total fragmentation cross section (for $Z \geqslant 3$) will be published at a later time. While no total reaction cross section data exist at this time in the 100 MeV/A range, accurate measurements exist at 2.1 GeV/A and a continuation formula is used to estimate the total reaction cross sections at 100 MeV/A. (Paul J. Karol, Phys. Rev. C11, 1203 (1975)). Needless to say the variation with energy is expected to be small, the cross sections being essentially geometric at both energies.

8. J. Gosset, H. H. Gutbrod, W. G. Meyer, A. M. Poskanzer, A. Sandoval, R. Stock, G. D. Westfall, Phys. Rev. C16, 629 (1977). We thank D. Morrissey for the help with the fireball geometry calculations.

9. C. K. Gelbke, D. K. Scott, M. Bini, D. L. Hendrie, J. L. Laville, J. Mahoney, M. C. Mermaz, C. Olmer, Phys. Lett. 70B, 415 (1977).

Table I. Summary of the fitted parameters σ_1, σ_2 of Eq. (2) to the experimental $\sigma_{p_\perp}$. These are compared with our calculated values of σ_2 for f = 0.6 and $R = r_o(A_1^{1/3} + A_2^{1/3})$, r_o = 1.2 fm; a = 0.6 fm and V tabulated.

TARGET	$E_{lab}(^{16}O)$ (MeV/A)	σ_1	$\sigma_{2\ exp}$ (MeV/c)	$\sigma_{2\ th.}$	V (MeV)
Al	92.5	80	248.6±2.3		
		86	241.4±2.4		
		84.4±2.2[a]	243.4±3.5	197.2	60[b]
Au	92.5	80	227.3±3.8		
		86	219.9±3.9		
		83.7±3.5[a]	222.8±5.8	193.6	85[b]
Al	117.5	80	227.2±2.6		
		86	219.3±2.7		
		92.1±2.3[a]	210.6±4.4	174.9	60
Au	117.5	80	214.2±4.0		
		86	206.4±4.1		
		84.0±3.8[a]	209.1±6.5	169.6	85

a) two parameter fit; σ_1 unconstrained.

b) V determined to reproduce the angular distributions at 92.5 MeV/A.

FIGURE CAPTIONS

Fig. 1. Typical angular distributions for ^{16}O+Al, ^{16}O+Au at 92.5 MeV/A. The solid curves are the best fit from Eq. (1); the dashed curves for $\sigma_{p_\perp}$ = 86 MeV/c. The dotted curves result from folding the deflection function with the momentum distribution due to the intrinsic nucleon motion; the fine lines similarly, but under the abrasion-ablation assumption.

Fig. 2. Observed $\sigma_{p_\perp}$ for each isotope for (a) ^{16}O+Al, 117.5 MeV/A, (b) ^{16}O+Au, 117.5 MeV/A, (c) ^{16}O+Al, 92.5 MeV/A; (d) ^{16}O+Au, 92.5 MeV/A. For panels (a)-(c), the fitted curves are the best two-parameter fit (σ_1 and σ_2 both unconstrained; values fround in Table I); curves in panel (d) are for σ_1 = 83.7 MeV/c; values of σ_2 from 0 to 300 MeV/c to show the presumed evolution of $\sigma_{p_\perp}$ as one goes from the extreme relativistic case to lower energies where the orbital dispersion of the projectile becomes significant.

Fig. 3. Calcualted deflection functions, Θ (b) for ^{16}O+Al, ^{16}O+Au at 92.5 MeV/A. Insert shows the relevant range in impact parameter for fragmentation, as determined from a sharp cutoff model, subject to the condition that $\sigma_{frag}/\sigma_{tot}$ = 0.6.

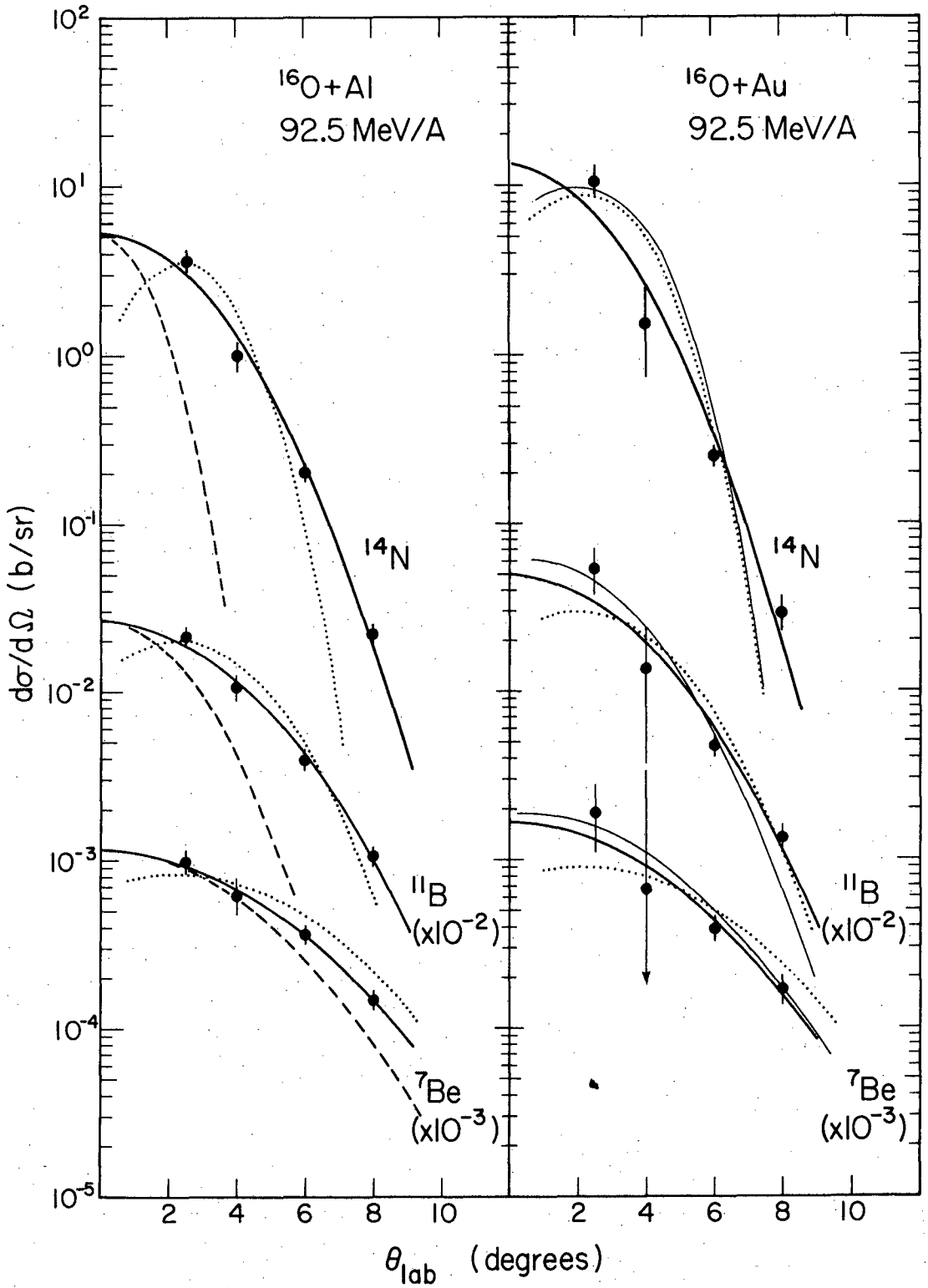
^{16}O+Al
92.5 MeV/A
^{16}O+Au
92.5 MeV/A
^{14}N
^{11}B
(x10^{-2})
^{7}Be
(x10^{-3})
dσ/dΩ (b/sr)
θ$_{lab}$ (degrees)
XBL 791-301

Fig. 1

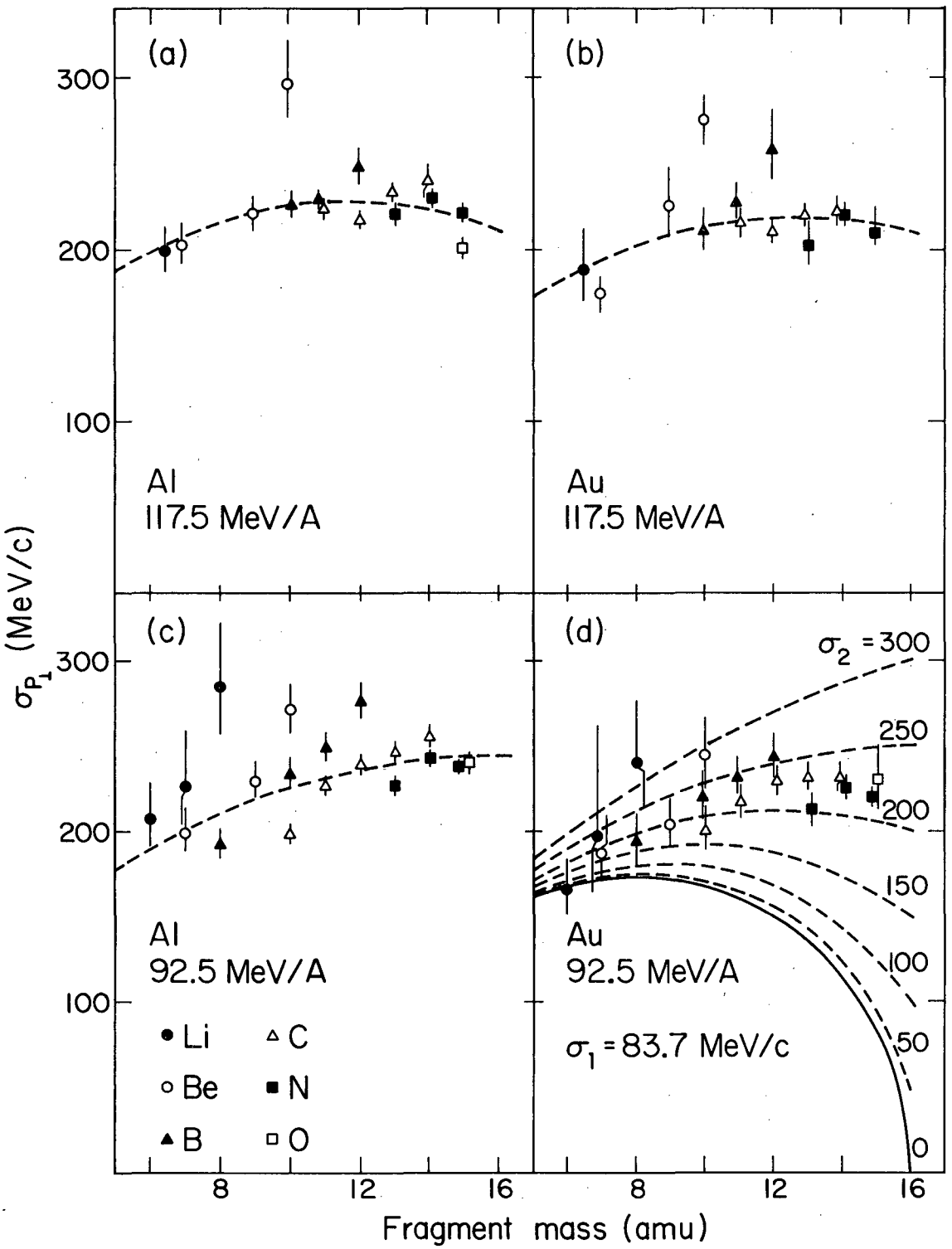
(a)
(b)
(c)
(d)
Al
117.5 MeV/A
Au
117.5 MeV/A
Al
92.5 MeV/A
Au
92.5 MeV/A
σ1 = 83.7 MeV/c
σ2 = 300
250
200
150
100
50
0
Li
C
Be
N
B
O
σP1 (MeV/c)
Fragment mass (amu)
XBL791-103

Fig. 2

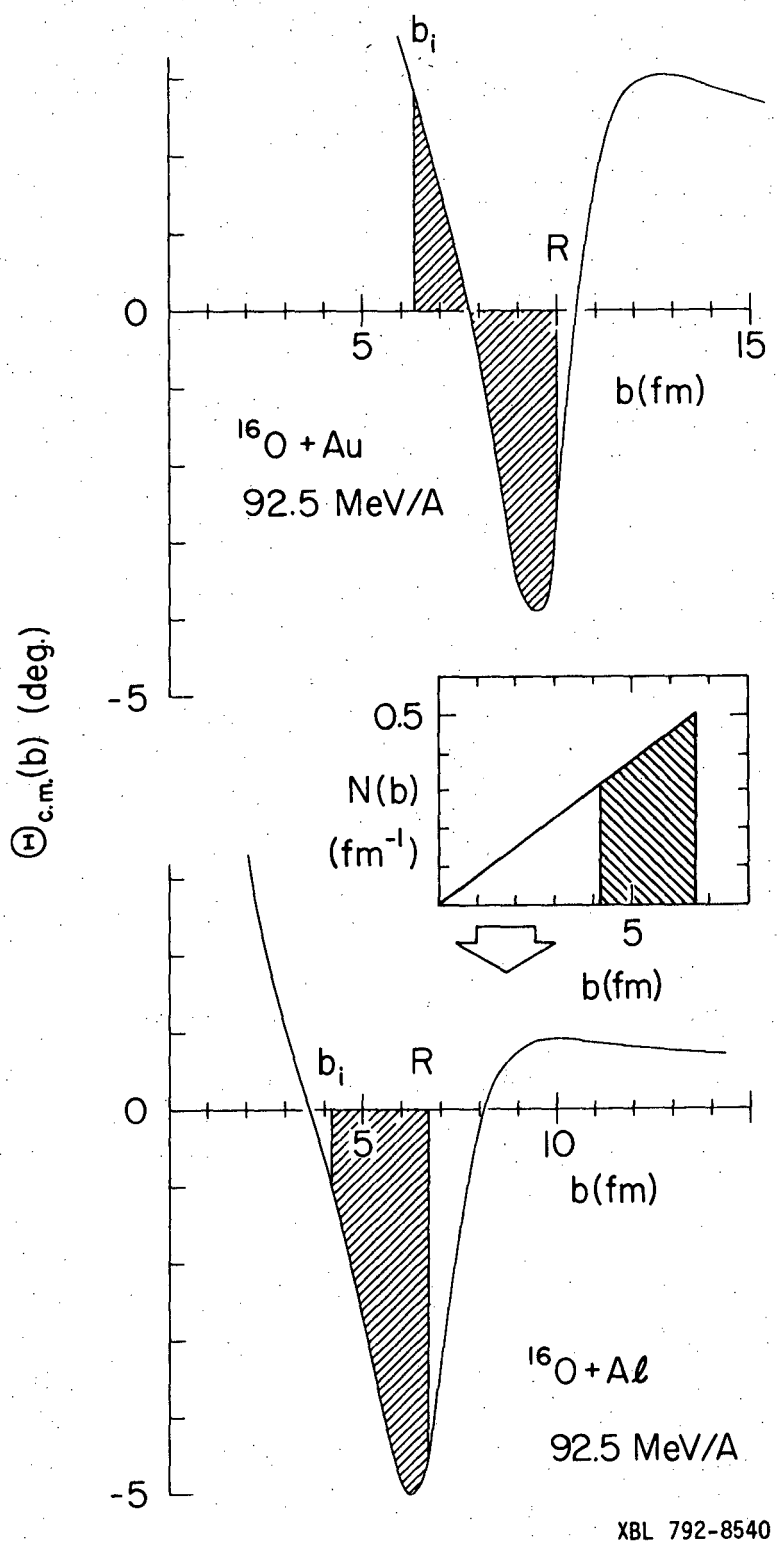
b_i
R
0
5
15
b(fm)
$^{16}O + Au$
92.5 MeV/A
-5
$\Theta_{c.m.}(b)$ (deg.)
0.5
N(b)
(fm^{-1})
5
b(fm)
b_i
R
0
5
10
b(fm)
$^{16}O + Al$
92.5 MeV/A
-5
XBL 792-8540

Fig. 3

TECHNICAL INFORMATION DEPARTMENT
LAWRENCE BERKELEY LABORATORY
UNIVERSITY OF CALIFORNIA
BERKELEY, CALIFORNIA 94720